Advances in Water Resources 000 (2017) 1–9

Contents lists available at ScienceDirect

Advances in Water Resources

journal homepage: www.elsevier.com/locate/advwatres

Using modal decompositions to explain the sudden expansion of the mixing layer in the wake of a groyne in a shallow flow

J.E. Higham[a,*], W. Brevis[a], C.J. Keylock[a], A. Safarzadeh[b]

[a] Department of Civil and Structural Engineering, University of Sheffield, Sheffield, U.K
[b] Department of Civil Engineering, University of Mohaghegh Ardabili, Ardabili, Iran

ARTICLE INFO

Article history:
Received 21 December 2016
Revised 24 April 2017
Accepted 16 May 2017
Available online xxx

Keywords:
Dynamic mode decomposition
Proper orthogonal decomposition
Shallow flow
Groyne
Spur dyke

ABSTRACT

The sudden expansion of the mixing layer created in the wake of a single groyne is investigated using Particle Image Velocimetry (PIV). In the region of the sudden expansion a patch of high Reynolds shear stresses are observed. Using low-order representations, created from a Dynamic Mode Decomposition and a search criteria based on a Proper Orthogonal Decomposition, the spatio-temporal mechanism of the sudden expansion is investigated. The present study demonstrates the sudden expansion is created by the periodic merging of eddies. These eddies originate from the upstream separation and the tip of the groyne and merge with recirculating eddies created, downstream of the groyne, at the interface of the mixing layer and the lateral wall.

1. Introduction

In natural flows such as rivers and estuaries, groynes are installed to prevent bank scouring (Przedwojski, 1995; Sukhodolov et al., 2002) or to create and enhance fish habitats (Grift et al., 2003). The majority of these natural flows are bounded flows in a domain for which two dimensions, namely that in the direction of the flow, as well as one traverse dimension, greatly exceed the third dimension, consequently they fulfil definition of a shallow flow (Jirka, 2004).

Dependent upon the magnitude of the transversal velocity gradient, a topographical obstruction of any flow can lead to the formation of a mixing layer. In contrast to in deep flows, the large-scale coherent turbulent structures which populate the far field of a shallow mixing layer, can almost extend the whole depth of the flow. As a consequence these quasi-two-dimensional coherent structures (Q2CS), and their spatio-temporal dynamics, are easily influenced by bed-friction (Chu and Babarutsi, 1988; Nadaoka and Yagi, 1998; Socolofsky and Jirka, 2004; Uijttewaal and Tukker, 1998). From an environmental perspective these Q2CS are of great significance, as their spatio-temporal behaviour governs mass and momentum exchange. Some examples of this can be found in their key role to predict the concentration of pollutants, nutrients and the rates of sediment transport (Boyer et al., 2006; Cheng and Constantinescu, 2014; Rhoads and Sukhodolov, 2004; Sukhodolov and Rhoads, 2001).

Many previous works have investigated the spatio-temporal dynamics of Q2CS created by plane shear instabilities e.g. (Chu and Babarutsi, 1988; Rhoads and Sukhodolov, 2004; Uijttewaal and Tukker, 1998), and have shown that due to the effects of bed-friction the spread/growth rate of a shallow mixing layer is modified. In an experimental study to investigate the effect of topographical forcing on a shallow flow, Talstra et al. (2006) found that unlike in a deep flow, (Armaly et al., 1983), the shallow flow mixing layer bound a second counter rotating recirculation cell. They also found at the downstream edge of the first recirculation cell there was a sudden expansion in the mixing layer. In Talstra (2011) it is suggested that this sudden expansion is caused by the merging of vortex shed from the tip of the obstacle and those associated to the largest downstream gyre. In a more recent study, this sudden expansion was also found to occur when a shallow flow was obstructed by a single lateral groyne, it was also observed that the length of reattachment of the mixing layer with the wall was protracted compared with the a deep case (Safarzadeh and Brevis, 2016; Safarzadeh et al., 2016). A number of time-averaged experimental studies have previously investigated this case, but have neither observed or explained this phenomena (Ahmed et al., 2010; Duan et al., 2009; Francis et al., 1968; Kadota and Suzuki, 2010). The Reynolds Averaged Navier–Stokes (RANS k-ω) simulations of Chrisohoides et al. (2003) observed the dual cell system and found that it was stable but periodically horizontally expand-

* Corresponding author.
E-mail address: jhigham1@sheffield.ac.uk (J.E. Higham).

http://dx.doi.org/10.1016/j.advwatres.2017.05.010

ing and contracting. They further found that eddies from upstream and shed from the tip of the obstacle were engulfed by the second downstream recirculation cell, and as the mixing layer reattached with the lateral wall, vorticity was injected back upstream; however they did not observe a sudden expansion the mixing layer. Safarzadeh and Brevis (2016) recently explained that due to the anisotropy associated to the flow system, RANS simulations, based on isotropic closure models, will not be able to simulate the expansion of the mixing layer or predict the length of reattachment. Other Computational Fluid Dynamics (CFD) studies relating to a single groyne have only focused on the turbulent mechanisms upstream and in the near wake of the groyne e.g. (Garde et al., 1961; Koken, 2011; Koken and Constantinescu, 2008; 2009; Paik and Sotiropoulos, 2005), whilst not directly related to this study it is inferred that these complexities have implications on the dynamics of the mixing layer downstream. From all of these findings it is clear that the dynamics of a shallow mixing layer produced in the downstream wake of a single groyne are complex and governed by a number of factors.

The main goal of this research is to investigate the spatio-temporal mechanisms and Q2CS relating to the sudden expansion of the mixing layer. Whilst, the occurrence of this has been previously observed, the physics leading to it has not. Such an interpretation of the physics is important, as this understanding will help one to hypothesise how different flow and boundary conditions will affect the formation and dynamics of the sudden expansion. This is particularly important from an environmental perspective as the increased moment fluxes relating to this phenomenon can lead to enhanced scouring/mixing processes. To investigate these mechanisms an experimental Particle Image Velocimetry (PIV) study is undertaken. To describe the spatio-temporal mechanism a low-order reconstruction of the flow is made from the temporally orthogonal Dynamic Mode Decomposition (DMD) (Rowley et al., 2009; Schmid, 2010) using on a search criteria based on a spatially orthogonal Proper Orthogonal Decomposition (POD) (Aubry, 1991; Berkooz et al., 1993).

2. Experimental setup

An experimental investigation was undertaken at the Karlsruhe Institute of Technology in a tilting 18 m × 1.82 m shallow water flume, a sketch of which is shown in Fig. 1. The flume's bottom and sidewalls are coated in a black plastic laminate. A single obstacle constructed from aluminium plate measuring 0.25 × 0.05 × 0.05 m was placed perpendicular to and at the wall of flume 12 m from the channel entrance. The flow rate Q was set to 13.5 ls^{-1}, and the flume slope inclined to 0.1 mm/m with a water depth H=0.04 m. The Reynolds number was set at, $\mathrm{Re} = \rho U_0 H/\nu$=29,680, where U_0, ρ and ν are the bulk flow velocity, water density, dynamic viscosity, with a sufficiently low Froude number, $\mathrm{Fr} = U_0/\sqrt{gh} = 0.29$, where g is the acceleration of gravity, to ensure minimal surface disturbances as shown by Uijttewaal (2005). To capture the large-scale turbulent structures, a planar Particle Image Velocimetry (PIV) measurement system was used. The PIV system consisted of an industrial grade camera with a 1200 × 1200 CCD-sensor with 12 bit resolution. The flow was seeded with floating 2.5 mm hexagonal polyester particles using a pneumatic particle dispenser. In a shallow flow floating particles have previously been shown to be effective in capturing the large scale turbulent motions by Weitbrecht et al. (2002). The camera was mounted directly above the water surface at a height of 1.5 m and was set to capture an area of 150 × 45 cm with 5 cm overlapping between upstream and downstream images. Measurements were conducted in eight consecutive planes, one upstream of the obstacle and seven downstream. In each position snapshots were recorded at an acquisition frequency of 37 Hz. The image sequence was analysed using the PIV package for Linux GPIV (van der Graaf, 2010), using multi-pass and image deformation techniques. As discussed by Huang et al. (1997) digital PIV often has an associated error, this error can be associated to the seeding distribution. The work of Higham et al. (2016) also shows outlier vectors can increase this error. In the present study it is estimated these errors are approximately 4%. To reduce the influence of the outlier error the PODDEM algorithm (Higham et al., 2016) was implemented.

3. Proper orthogonal decomposition

POD is a linear statistical method commonly used in fluid mechanics for the extraction and analysis of energy meaningful turbulent structures (Aubry, 1991; Berkooz et al., 1993). POD was independently derived by a number of individuals, and consequently takes a variety of names in different fields such as Karhunen-Loève Decomposition, Singular Value Decomposition (SVD) and Principal Components Analysis (PCA) (Karhunen, 1946; Kosambi, 1943; Loève, 1945; Obukbov, 1954; Pougachev, 1953). A POD extracts the most relevant modes from set of a stochastic signal. In fluid mechanics a POD is typically applied to a set of snapshots, which can be obtained from a computer simulation or experimental data typically with two or three components. The POD is used to determine spatially orthogonal energy relevant structures from statistically steady-state turbulent fields, within a finite time domain, ordering them by their contribution to the total variance of the physical property being analysed, e.g. intensity (Brevis and García-Villalba, 2011). A set of $t = 1, 2, \ldots, T$ temporally ordered snapshots, $\mathbf{V}(x, y; t)$, is considered, each of which is of dimension $X \times Y$. The method requires the construction of an $N \times T$ matrix $\mathbf{W}$ from T columns, $\mathbf{w}(t)$ of length $N = XY$, each one corresponding to a column-vector version of a transformed snapshot $\mathbf{V}(x, y; t)$. A POD can be obtained by :

$$\mathbf{W} \equiv \mathbf{\Phi S C}^{*} \tag{1}$$

where $\mathbf{S}$ is the singular valies matrix of dimension $\Theta \times \Theta$, (Θ are the number of modes of the decomposition, and $(\cdot)^*$ represents a conjugate transpose matrix operation). The $\lambda = \mathrm{diag}(\mathbf{S})^2/(N-1)$ is the vector containing the contribution to the total variance of each mode. The elements in λ are ordered in descending rank order, i.e. ($\lambda_1 \geq \lambda_2 \geq \cdots \lambda_\Theta \geq 0$). In practical terms the matrix $\mathbf{\Phi}$ of dimension $N \times \Theta$ contains the spatial structure of each of the modes and the matrix $\mathbf{C}$ of dimension $\Theta \times \Theta$ contains the coefficients representing the time evolution of the modes. Furthermore, the percentage turbulent kinetic energy contribution, E, of a each POD mode can be obtained via:

$$E(\%) = \frac{\lambda_i}{\sum_{i=1}^{N}} \cdot 100 \tag{2}$$

4. Dynamic mode decomposition

The Dynamic Mode Decomposition (DMD) algorithm was introduced into fluid mechanics by Schmid (2010) & Rowley et al. (2009), based on a Arnoldi Eigenvalue algorithm suggested by Ruhe (1984). Unlike POD, which is based upon a co-variance matrix, using and Arnoldi approximation the DMD fits a high-degree polynomial to a Krylov sequence of snapshots, which are assumed to become linearly dependent after a sufficient number of snapshots (Mezić, 2005; Schmid et al., 2009). As discussed by Schmid (2011) such a representation of a nonlinear process by a linear sample-to-sample map can be closely linked to the concept of a Koopman operator, an analysis tool for dynamical systems. For complex flow systems containing superpositions of turbulent structures and mechanisms, the DMD algorithm can be used to extract spatial modes with single 'pure' frequencies. There are currently

Please cite this article as: J.E. Higham et al., Using modal decompositions to explain the sudden expansion of the mixing layer in the wake of a groyne in a shallow flow, Advances in Water Resources (2017), http://dx.doi.org/10.1016/j.advwatres.2017.05.010

a number of methods by which one can compute a DMD, and the method used in the present study is the popular SVD based method; this approach has been shown to be less susceptible to experimental noise (Schmid, 2010). The algorithm is outlined below, although the reader is directed to Jovanović et al. (2014); Schmid (2010); Tu et al. (2013) for the full mathematical description. The DMD algorithm begins with a similar transformation as POD:

$$\mathbf{W^A} = \{w_1, w_2, \ldots, w_\tau\}, \quad \text{and} \quad \mathbf{W^B} = \{w_2, w_3, \ldots, w_T\} \tag{3}$$

where $\tau = (T-1)$, and the super-scripts A and B denote the two $\mathbf{W}$ matrices of dimension $N \times \tau$. A SVD of $\mathbf{W^A}$ is computed, such that:

$$\mathbf{W^A} \equiv \tilde{\mathbf{\Phi}}\tilde{\mathbf{S}}\tilde{\mathbf{C}}^*. \tag{4}$$

where $\tilde{\mathbf{\Phi}}, \tilde{\mathbf{S}}$ and $\tilde{\mathbf{C}}$ are the POD modes, the singular values and the temporal coefficients of $\mathbf{W^A}$ respectively. The matrix $\mathbf{F}$, of dimension $(\tau \times \tau)$, is created by:

$$\mathbf{F} = \tilde{\mathbf{\Phi}}\mathbf{W^B}\tilde{\mathbf{C}}\tilde{\mathbf{S}}^{-1} \tag{5}$$

and its complex Eigenvalues, μ_i, and Eigenvectors, z_i, are computed where $i = 1 \ldots \tau$. At this point the method of Jovanović et al. (2014) is used, as this creates a set of amplitudes for each spatial mode. Following Jovanović et al. (2014) a Vandermonde matrix is created from the complex eigenvalues:

$$\mathbf{Q}_{i,j} = \mu_i^{(j-1)} \tag{6}$$

where $i = 1 \ldots \tau$ and $j = 1 \ldots \tau$, and the spatial modes are created by $\mathbf{\Psi} = \tilde{\mathbf{\Phi}}\mathbf{Z}$, where $\mathbf{Z}$ is a matrix of complex Eigenvectors previously computed. Furthermore, a matrix of amplitudes, $\mathbf{D_\alpha}$, are created and the original input, $\mathbf{W^A}$, can be expressed as:

$$\mathbf{W^A} \equiv \mathbf{\Psi}\mathbf{D}_\alpha\mathbf{Q} \tag{7}$$

where $\mathbf{D_\alpha}$ is of dimension $\tau \times \tau$. $\mathbf{\Psi}$, is a matrix of dimension $N \times \tau$ containing the DMD spatial modes. $\alpha = diag(\mathbf{D}_\alpha)$ relates to their amplitude $\mathbf{\Psi}$, but not their variance, and $\mathbf{Q}$ contains the coefficients representing the time evolution of the modes. In practical terms, as shown by Chen et al. (2012) the angle between the real and imaginary part of, z_i, can be used to describe the frequency relating to each $\mathbf{\Psi}$ and expressed as a Strouhal number by:

$$\mathrm{St}_i = (2\pi \mathrm{U}_0 \arg\{z_i\})/(f_0 \mathrm{L}) \tag{8}$$

where, $i = 1 \ldots \tau$, L is the length of the groyne and U_0 is the bulk velocity and f_0 is the acquisition frequency.

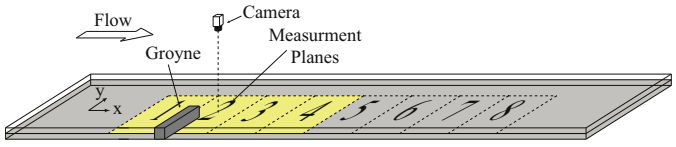

Fig. 1. Sketch of the experimental setup (not to scale).

5. Results

5.1. Time-averaged statistics

As previously outlined, the emphasis of the present work is to describe the mechanisms underpinning the sudden expansion of the mixing layer. Before investigating the spatio-temporal mechanisms, time-averaged statistics are used to find its location and investigate any related turbulent properties. Time-averaged statistics are created separately from 8 PIV planes, each obtained from 21,000 snapshots, these planes are highlighted in Fig. 1. The co-ordinate system is normalised by the length of the groyne, L, and the axes are termed x/L and y/L. The co-ordinate system originates in the x-direction at the centre of the groyne and in the y-direction where the groyne meets the wall. The data obtained are two component snapshots u (x-direction) and v (y-direction), see Fig. 1, where $\langle\cdot\rangle$ denotes time-average. Fig. 2 presents a time-

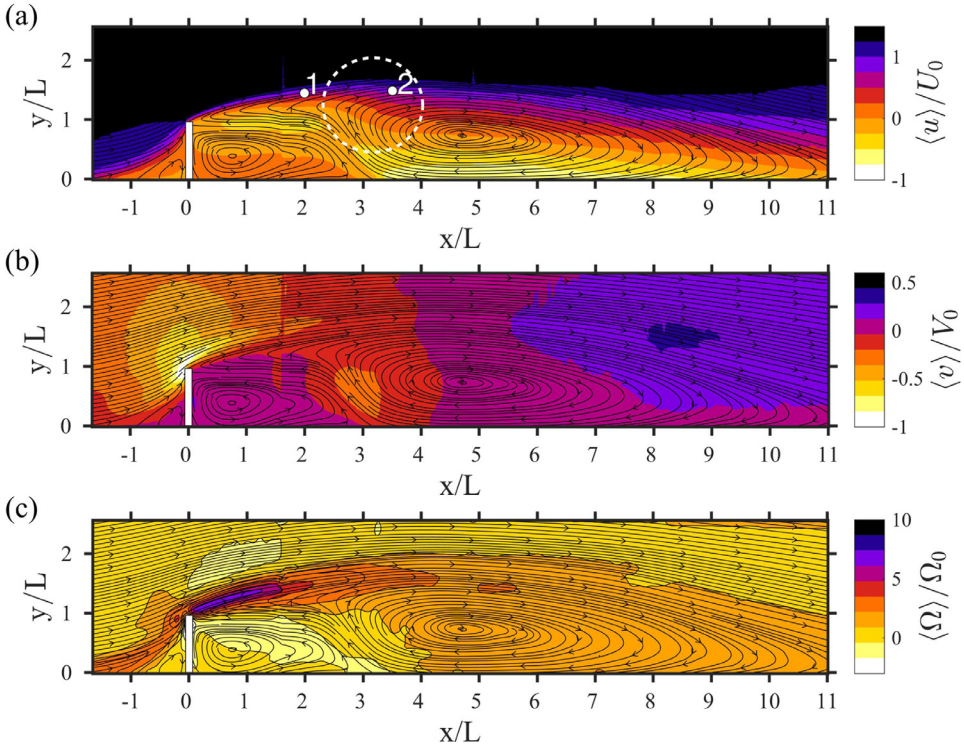

Fig. 2. Mean statistics created from eight overlapping planes. (a) Shows the time averaged streamwise velocity, (b) shows the time averaged spanwise velocity, (c) shows the time averaged vorticity. The white dashed circle in (a) highlights the location of the sudden expansion of the mixing layer. All contour plots have mean streamlines overlaid.

Please cite this article as: J.E. Higham et al., Using modal decompositions to explain the sudden expansion of the mixing layer in the wake of a groyne in a shallow flow, Advances in Water Resources (2017), http://dx.doi.org/10.1016/j.advwatres.2017.05.010

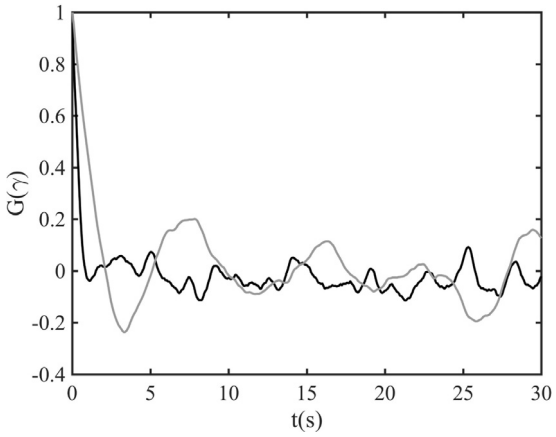

Fig. 3. Streamwise autocorrelation function, G(γ), taken at two points, before and after sudden expansion. The location of the points chosen are plotted on Fig. 2(a). Black line relates to (1) (before expansion) and (2) grey line relates to 2 (after expansion).

averaged overview of the flow system, where (a) shows the time averaged streamwise velocity component normalised by the bulk velocity U_0, (b) shows the time averaged spanwise velocity component normalised by the bulk velocity U_0 and (c) shows vorticity, $\Omega = (\partial u/\partial y - \partial v/\partial x)$ (i.e. the bottom wall normal component), normalised by its spatial-temporal average, Ω_0. All figures are overlaid by the mean streamlines.

As shown in Fig. 2 as the flow approaches the groyne it separates. The separation of the flow creates a mixing layer bounding two counter rotating recirculation zones, which reattaches with the lateral wall at $x/L\sim$ 11. The first counter-clockwise rotating recirculation cell extends the whole spanwise length of the obstacle (y/L= 1) and three obstacle lengths downstream (x/L= 3). The second downstream recirculation cell is clockwise rotating and originates from the tip of the obstacle. Due to the first downstream recirculation cell, this cell does not meet the lateral wall until x/L= 3. The interface between these two recirculation cells and the mixing layer is located around the same point as the sudden expansion (highlighted in Fig. 2(a) by a white circle). The sudden expansion is further shown to occur in the streamwise autocorrelation function in Fig. 3 (the locations of the two chosen points are highlighted in Fig. 2(a)). Where the autocorrelation function is defined as:

$$G(\gamma) = \frac{\langle u(t)u(t+\gamma)\rangle}{\langle u^2\rangle} \tag{9}$$

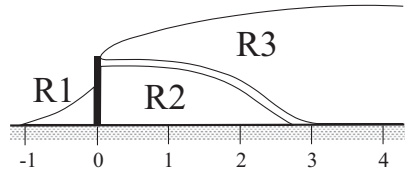

Fig. 4. Nomenclature of recirculation zones.

where $\gamma = t_{i+1} - t_i$. From the streamwise autocorrelation function the sudden expansion is clearly highlighted by a jump in length of the integral time scales, before and after the sudden expansion. As shown Fig. 2(c), eddies shed from the tip of the obstacle create a region of high vorticity. In this region the vorticity reaches a maximum at x/L= 1.2 and is sustained up until x/L= 3. At this point the concentration becomes less, and finally by $x/L\sim$ 4 the region of high vorticity is no longer visible.

The focus now concentrates on the first four planes, as this corresponds to the location of the sudden expansion of the mixing layer (as discussed in Section 1). These planes are highlighted in yellow in Fig. 1. A nomenclature for the recirculation cells is also introduced, as shown in Fig. 4. The upstream recirculation zone is termed R1, the first downstream recirculation zone is termed R2 and the second downstream recirculation zone is termed R3. In Fig. 5 (a–c) contour plots of the Reynolds stresses $\langle u'u'\rangle$, $\langle v'v'\rangle$ & $\langle u'v'\rangle$ (where $u = \langle u\rangle + u'$ etc.) normalised by U_0^2, and (d) contour plots of the turbulent kinetic energy, TKE=$(\langle u'^2\rangle + \langle v'^2\rangle)/2$ by U_0 are plotted. The $\langle u'v'\rangle$ contour plots show along the mixing layer, between x/L= 2 and x/L= 4 an intense patch of momentum fluxes. The centre of this intense region $x/L\sim$ 3, $y/L\sim$ 1.7, coincides with the point at which the concentration of TKE begins to decrease. From the $\langle u'u'\rangle$ and $\langle v'v'\rangle$ contour plots, it is evident that the patch seen in $\langle u'v'\rangle$ relates the change in direction of the momentum fluxes. From these plots it can be concluded that in this region a process is occurring leading to the sudden expansion of the mixing layer. To investigate the spatio-temporal mechanism responsible for this phenomenon, the modal decompositions described earlier are used to extract the primary features of interest from the complex dynamics observed in this region.

5.2. Modal decompositions

A Proper Orthogonal Decomposition is computed using 7000 fluctuating snapshots. Only a subset is chosen due to computational limitations (which is equivalent to 30 integral time scales

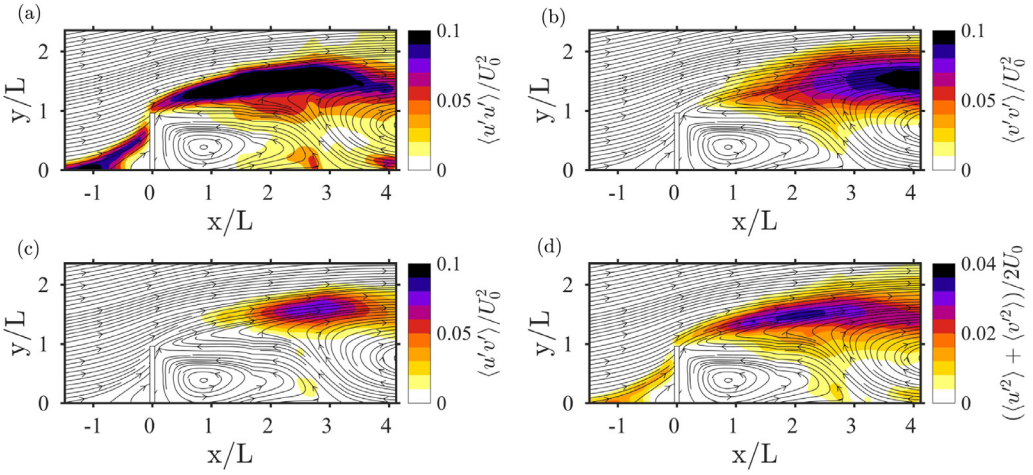

Fig. 5. (a–c) Reynolds shear stresses $\langle u'u'\rangle/U_0^2$, $\langle v'v'\rangle/U_0^2$ & $\langle u'v'\rangle/U_0^2$ respectively (d) Turbulent kinetic energy $(\langle u'^2\rangle + \langle v'^2\rangle)/2U_0$.

Please cite this article as: J.E. Higham et al., Using modal decompositions to explain the sudden expansion of the mixing layer in the wake of a groyne in a shallow flow, Advances in Water Resources (2017), http://dx.doi.org/10.1016/j.advwatres.2017.05.010

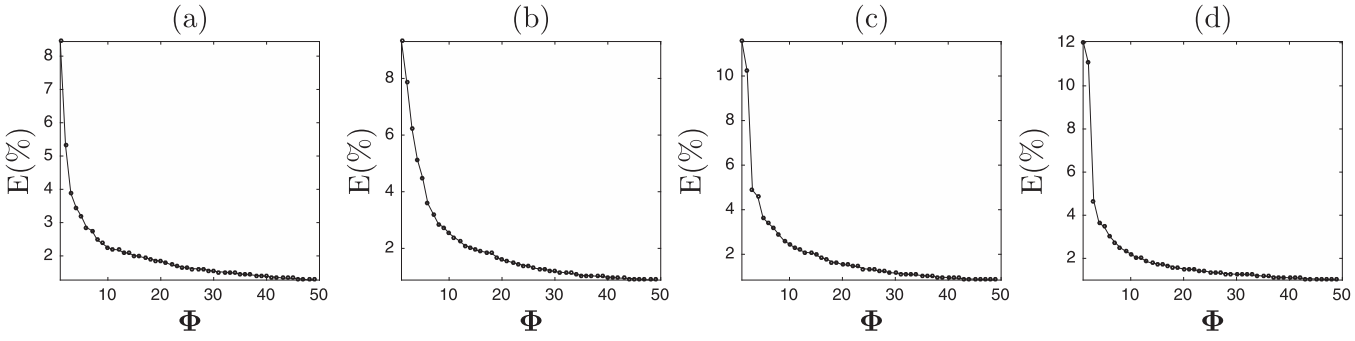

Fig. 6. POD spectra where $\lambda = diag(\mathbf{S})$, these values represent each spatial modes $\mathbf{\Phi}_i$ contribution to the total variance.

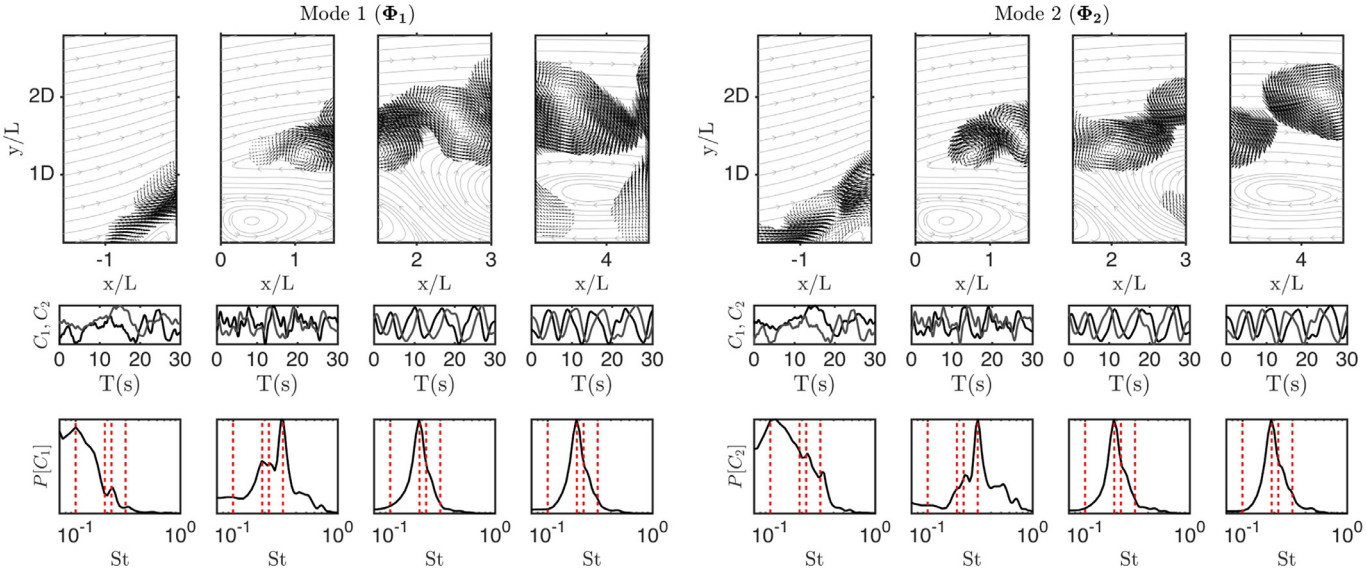

Fig. 7. POD modes ($\mathbf{\Phi}_1$ & $\mathbf{\Phi}_2$) obtained from a Proper Orthogonal Decomposition of four separate planes. The top row shows the spatial modes plotted using vector plots (with a threshold implemented to highlight the spatial structures). Underneath the POD modes the mean streamlines are plotted for reference. The middle row shows a small excerpt of the temporal coefficients (black depicts the current mode, and grey depicts the paired mode). Bottom row shows a power density spectrum created from the POD coefficients ($\mathbf{C}$). The red dashed link denote St=0.10, 0.19, 0.22, 0.31 respectively. (For interpretation of the references to colour in this figure legend, the reader is referred to the web version of this article.)

in the streamwise direction). The computation was undertaken on each of the four PIV planes independently. As shown in Fig. 6, the singular value, λ, which is computed as part of the POD can be used as a descriptor of a modes contribution to the total variance (i.e. turbulent kinetic energy). It is observed that on average the top four modes ($\mathbf{\Phi}_1$ & $\mathbf{\Phi}_2$) account for about 35% of the total variance of the flow. As a consequence it is a reasonable assumption that these four modes are likely to contain the most relevant information regarding the Q2CS structures.

In the top planes of Figs. 7 & 8 the spatial modes $\mathbf{\Phi}_{1...4}$ are presented. The modes alone present a coherent picture of the turbulent structures. As shown by Rempfer and Fasel (1994), Brevis and García-Villalba (2011) and Le Clainche et al. (2015) paired modes, with a similar energy contribution, show spatial and temporal shifted features, when the temporal coefficients are sinusoidal. From $\mathbf{\Phi}_1$ and $\mathbf{\Phi}_2$ a number observations made by Chrisohoides et al. (2003) can be verified. $\mathbf{\Phi}_1$ & $\mathbf{\Phi}_2$ show eddies being shed from the tip of the obstacle and being advected along the mixing layer before being engulfed by R3. Furthermore, in $\mathbf{\Phi}_3$ & $\mathbf{\Phi}_4$ it is evident that there is entrainment of eddies back upstream from the reattachment of the mixing layer. However, the poor suitability of the POD for this particular case, i.e. a complex non-linear flow, is highlighted in the middle panes of Figs. 7 & 8. As shown by Brevis and García-Villalba (2011), $\mathbf{C}$ relate to the temporal evolution of $\mathbf{\Phi}$. Consequently, while they provide a usefully summary of the spatial behaviour, they also contain multiple frequencies (the coefficients are not sinusoidal), suggesting that each spatial POD mode contains multiple scales of turbulent structures and are not temporally orthogonal. It is therefore suggested that single frequencies relating to each of these POD spatially orthogonal turbulent structures can be found by means of a Fourier analysis of the coefficients. Although as POD is region dependent the peak frequencies obtained from the POD coefficients will relate to this region, and therefore the peak frequencies obtained from different regions may differ in their energy contribution. Whilst often this is unavoidable in large scale experimental studies this should be taken into consideration when using this method. Eq. (8) also shows that single pure frequencies can be extracted from a DMD, thus one can use frequencies calculated from $\mathbf{C}$ to identify spatial DMD modes, $\mathbf{\Psi}$. As shown in the bottom panes of Figs. 7 & 8 there are a number of peak frequencies relating to $\mathbf{\Phi}_{1...4}$ St={0.10, 0.19, 0.22, 0.31}, (these frequencies are highlighted by red dashed lines).

Similar to the POD, the DMD was computed independently on the four separate planes each containing a smaller number of snapshots (700), separated at a greater δt, relating to an acquisition frequency of 7.4 Hz (relating to 15 integral time scale). Only 700 velocity field are selected here to mitigate against problems discussed by Wynn et al. (2013) that a spatial dimension much

Please cite this article as: J.E. Higham et al., Using modal decompositions to explain the sudden expansion of the mixing layer in the wake of a groyne in a shallow flow, Advances in Water Resources (2017), http://dx.doi.org/10.1016/j.advwatres.2017.05.010

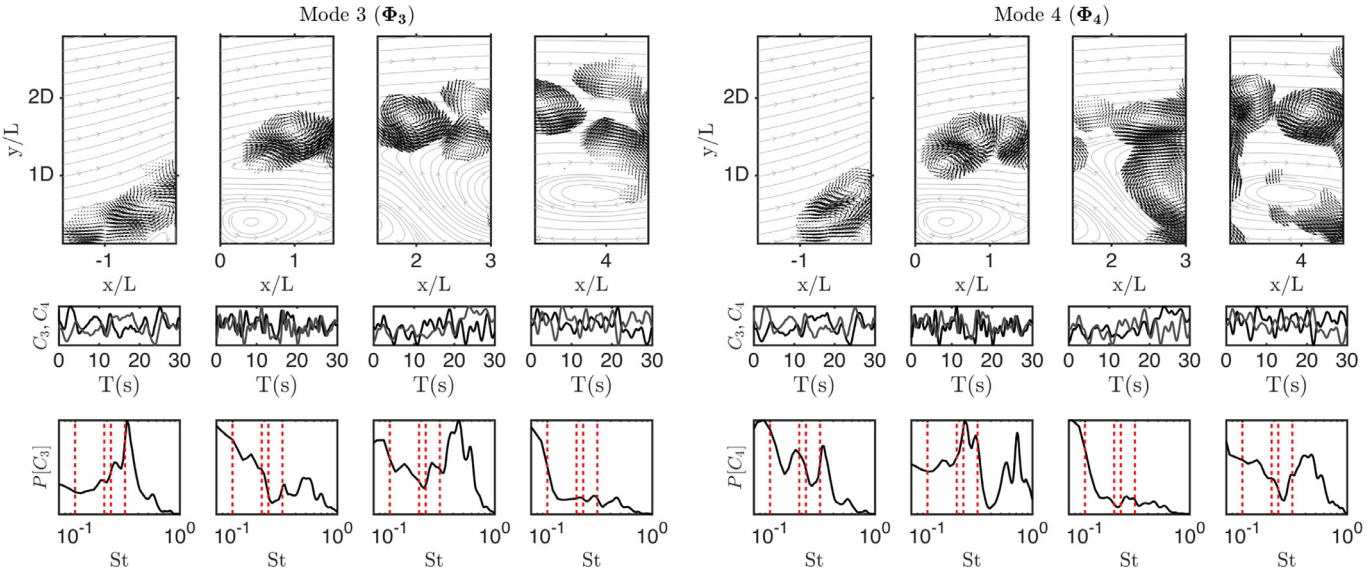

Fig. 8. POD modes (cont. from Fig. 7) ($\mathbf{\Phi}_3$ & $\mathbf{\Phi}_4$) obtained from a Proper Orthogonal Decomposition of four separate planes. The top row shows the spatial modes plotted using vector plots (with a threshold implemented to highlight the spatial structures), Underneath the POD modes the mean streamlines are plotted for reference. The middle row shows a small excerpt of the temporal coefficients (black depicts the current mode, and grey depicts the paired mode). Bottom row shows a power density spectrum created from the POD coefficients ($\mathbf{C}$). The red dashed link denote St=0.10, 0.19, 0.22, 0.31 respectively. (For interpretation of the references to colour in this figure legend, the reader is referred to the web version of this article.)

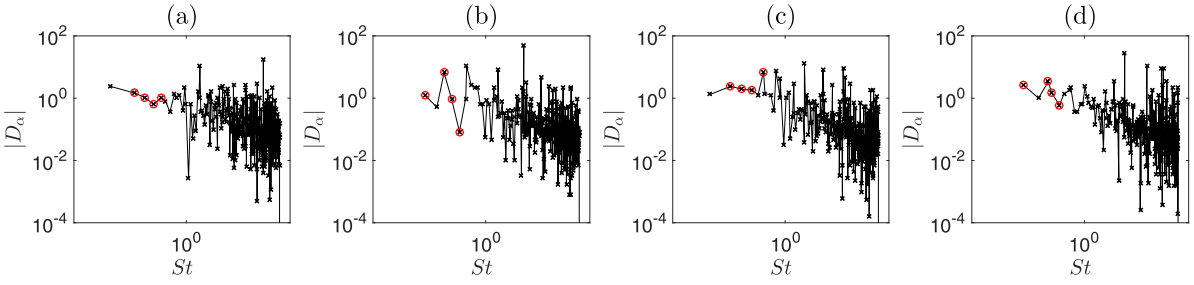

Fig. 9. The DMD spectra, based on the method of Jovanović et al. (2014). The x-axis relates to the Strouhal number of each spatial mode. The *y*-axis relates to the amplitudes, $\mathbf{D}_\alpha$, calculated in Eq. (7). The red circles highlight the spatial modes identified from the power spectrum of the POD temporal coefficients (St=0.10, 0.19, 0.22, 0.31). For the readers reference, the high frequency, high amplitude peaks in the spectra relate to experimental/background noise. (For interpretation of the references to colour in this figure legend, the reader is referred to the web version of this article.)

greater than the temporal dimension can result in an overfit of the data. The spectra associated to each DMD calculation are shown in Fig. 9, where the frequencies relating to the extracted POD modes are highlighted in red. For the reader's reference, whilst in these spectra it is apparent that they are higher frequencies with high amplitudes, the majority of these modes relate to noise, originating from the experimental data. Consequently highlighting that using a Fourier description based on a POD's temporal coefficients to select the spatial modes will mitigate against incorrectly choosing insignificant DMD modes with a high $\mathbf{D}_\alpha$, created by experimental/background noise. As shown by Brevis and García-Villalba (2011), and Rempfer and Fasel (1994), in a simple 'linear' case, a POD often determines conjugate pairs of modes, which spatially represent the advection of turbulent structures. As discussed by Schmid (2011) each DMD mode is complex (i.e. has a real and an imaginary component) and represents a linear process. In a DMD, analogous to a POD, the advection of the turbulent structures, can be seen between the real and imaginary parts of the complex DMD modes $\mathbf{\Psi}$. As shown in Fig. 10 the DMD modes offer a clean description of turbulence processes related to single frequencies, although it is difficult to deduce mechanisms regarding the sudden expansion of the mixing layer solely from the spatial modes. Nonetheless, as shown in Eq. 7 it is very simple to construct a low-order representation of the flow, because each reconstruction contains the same frequencies, it is also possible to create a time evolving coherent picture of the whole system. For illustration purposes the subsequent low-order planes are concatenated, but it is reiterated that the decompositions were reconstructed independently for each plane.

As shown by the reconstruction of the velocity vectors and velocity magnitude in Fig. 11 the size, dynamic and number of the recirculation cells is not static. Initially there are three recirculation cells, with R3 comprised of two cells, termed RC3a and RC3b as shown schematically in Fig. 12. As time progresses R3b expands and R2 simultaneously begins to stretch and split in two (R2a and R2b). The expansion of R3b causes the angle of the shear interface between the recirculation cells to periodically oscillate and the point of incidence of the shear layer and mixing layer to change. The region where the point of incidence moves about coincides with the high Reynolds stresses as seen in Fig. 5. This suggests that this mechanism of oscillation is associated with the sudden expansion of the mixing layer, as hypothesised by Talstra (2011), and Talstra et al. (2006). To investigate the turbulent structures associated with this mechanism, Fig. 13 shows a low-order reconstruction based upon the fluctuating vorticity, where dark grey is positive vorticity and light grey is negative vorticity. This figure demonstrates that it is the merging of two eddies that leads to the sudden expansion of the mixing layer. To highlight the pairing as

Please cite this article as: J.E. Higham et al., Using modal decompositions to explain the sudden expansion of the mixing layer in the wake of a groyne in a shallow flow, Advances in Water Resources (2017), http://dx.doi.org/10.1016/j.advwatres.2017.05.010

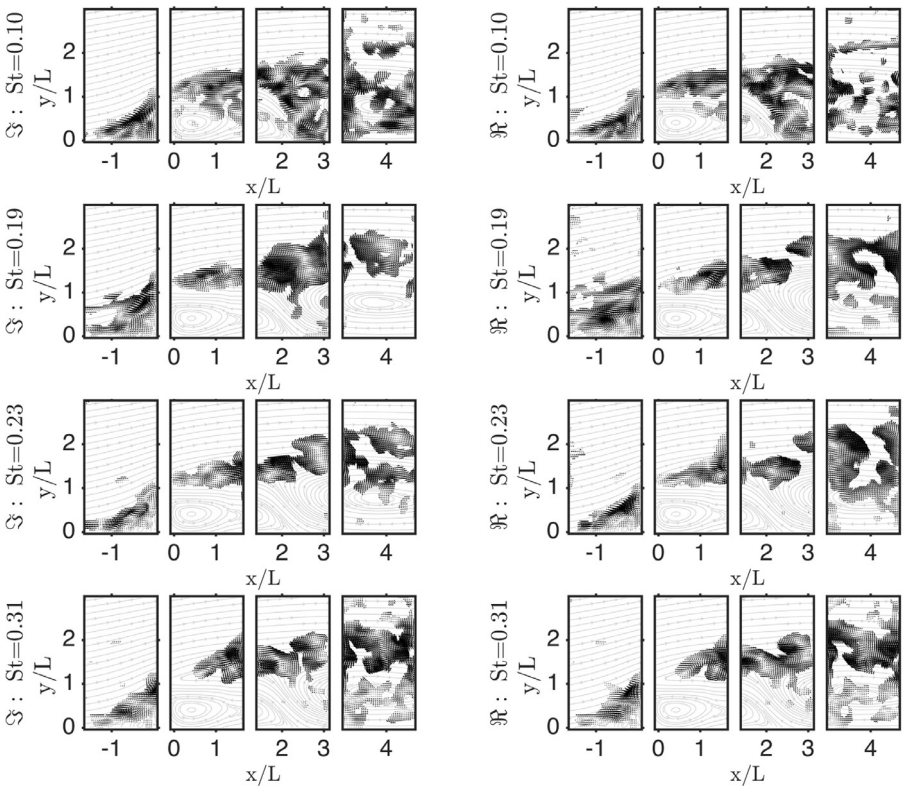

Fig. 10. DMD modes Ψ_{St}, where St relates to the modes Strouhal number. The left hand column shows the imaginary component and the right hand column the real component. The time averaged streamlines are plotted beneath as a reference. (St=0.10, 0.19, 0.22, 0.31).

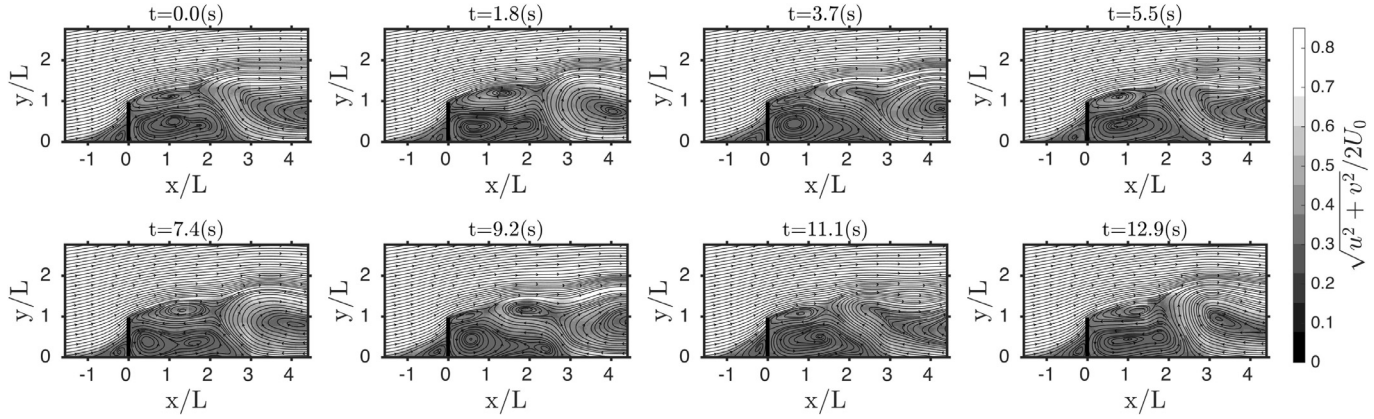

Fig. 11. A low-order reconstruction of velocity magnitude overlaid by streamlines, at selected temporal locations, including the mean flow field.

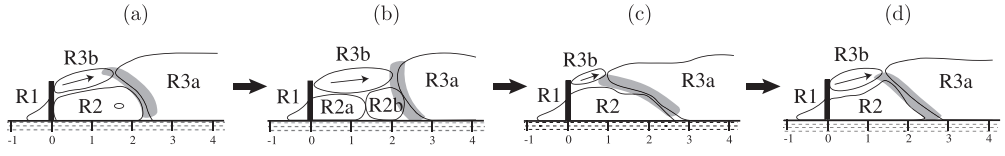

Fig. 12. Schematic of the turbulent mechanism underpinning the scale jump.

shown in Fig. 13, the two eddies are numbered (1) & (2). The first eddy (1) originates from upstream and the tip of the obstacle, the second (2) originates from vorticity injected upstream from the interaction of the mixing layer and the lateral wall. It is the constant injection of vorticity from upstream that leads to the formation of (2). Once this forms, it causes R3b to expand (explaining the periodic horizontal motion observed by Chrisohoides et al. (2003)). When (2) is sufficiently large enough it merges with (1) and advects along the mixing layer causing R3b to contract. This basic mechanism repeats itself periodically, leading to the observed dynamics, which have been documented for some time, but not previously explained satisfactorily.

6. Discussion

From the low-order reconstructions it is clear that the sudden expansion of the mixing layer is created by the pairing of two ed-

Please cite this article as: J.E. Higham et al., Using modal decompositions to explain the sudden expansion of the mixing layer in the wake of a groyne in a shallow flow, Advances in Water Resources (2017), http://dx.doi.org/10.1016/j.advwatres.2017.05.010

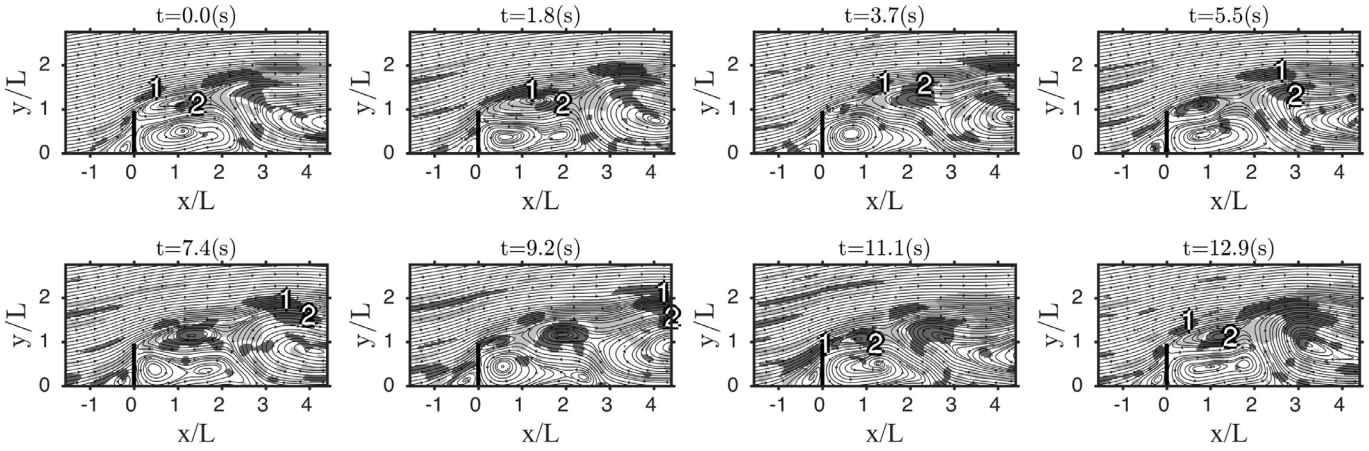

Fig. 13. A low-order reconstruction at selected points of the full turbulent mechanism. Dark grey indicates positive vorticity, light grey indicated negative vorticity.

dies, one created from the separation upstream and the tip of the obstacle and the other from the entrainment of vorticity, generated by impingement of the mixing layer and the wall. However, it is the interface between the two counter rotating recirculation cells that transports the second eddy into the mixing layer leading to the sudden expansion. It has previously been shown by Talstra (2011), Talstra et al. (2006) and Safarzadeh and Brevis (2016) that the shallowness of the flow leads to the production of the dual recirculation cell. The occurrence of the sudden expansion of the mixing layer is a function of the flow depth. Furthermore, previous works have shown how the effects of bed friction and the shallowness of the flow can affect the spatio-temporal dynamics of the turbulent structures/eddies (Chu and Babarutsi, 1988; Uijttewaal and Tukker, 1998). If the shallowness of the flow is decreased or the roughness is increased there will be an increase in the size of eddies and the point of reattachment with the wall will change, which will affect the location of the sudden expansion. Therefore the location of the sudden expansion of the mixing layer, and its occurrence, is a function of the shallowness of the flow and the roughness of the bed. The natural environment provides both shallowness and bed roughness, meaning that, in nature, the sudden expansion of the mixing layer is likely to occur. One example of this can be found in the work of Sukhodolov et al. (2010) where field measurements in the wake of a splitter plate show the that the effects of bed roughness can lead to a sudden expansion of a mixing layer. Whilst the present work is based upon laboratory experimental work, previous work has shown laboratory studies can be directly related to real flows (Le Coz et al., 2006). However, the determination of the degree of roughness or shallowness leading the occurrence and location of the sudden expansion of the mixing layer is beyond the scope of the present study.

Whilst the occurrence of this phenomenon would seem to be problematic due to the increased momentum fluxes at the point of impingement, in fact there are a number of benefits associated with this mechanism. For example, in the first downstream recirculation cell there are no large scale turbulent structures (see Fig. 13), i.e. a region in which momentum fluxes are minimal and a region not susceptible to erosion, sediment transport or mixing. This region therefore protects the near upstream region of the groyne and could offer a zone which could be beneficial for fish habitats and river restoration projects.

POD is well known in fluid mechanics and geophysics but relatively under-utilised in hydraulics, DMD is a new technique with a great deal of work on it in the last 7 years, and that the fusion of the two in the way done in the present study is a further contribution. As shown in the present study these methods can easily extract the large scale turbulent dynamics which govern a flow system. Whilst these methods may seem abstract, the processes which they are able to describe explain events which are of great significance in the mixing of pollutants, erosion and sediment transport. Furthermore, as shown in the present study, for complex systems with many intertwined turbulent processes, the Dynamic Mode Decomposition is able to describe these processes individually, something which could be used to create simplistic models of highly complex systems. These combination of these methods is also of a benefit for noisy data. As shown by Wang et al. (2015) low-order POD modes are unlikely to contain noise, therefore using low-order POD coefficients, as a search criterion, mitigates against the determination of noisy DMD modes. Although the present study is based on a highly accurate PIV technique, as shown by Brevis and García-Villalba (2011) this is not a requirement, and presented techniques could easily be applied data obtained from dye tracers/flow visualisations (Constantinescu et al., 2009).

7. Conclusions

Using a reconstruction of modes from a Dynamic Mode Decomposition and a selection criteria based on power spectrum obtained from the temporal coefficients of a Proper Orthogonal Decomposition the mechanism of the sudden expansion of the mixing layer is explained. The low-order representation, derived from the modes, reveals that eddies shed from the tip of the obstacle and those created upstream of the obstacle merge with eddies recirculated from the interaction of the mixing layer with the lateral wall, leading to the sudden expansion. Furthermore the present study suggests an alternative method for inferring flow structure from modal decomposition methods. The approach is to determine important frequencies from the temporal coefficients of a Proper Orthogonal Decomposition, which serve as a search criterion for choosing the modes from a Dynamic Mode Decomposition. The latter are then used to build a low-order model of the dynamics, from which process mechanisms may be inferred.

Acknowledgements

The first author was supported by a PhD studentship from the UK Natural Environment Research Council (NE/L501682/1). The second author was supported by Engineering and Physical Sciences Research Council (EP-L026457-1). The third author was supported by Royal Academy of Engineering/Leverhulme Trust Senior Research Fellowship (LTSRF1516-12-89).

References

Ahmed, H.S., Hasan, M.M., Tanaka, N., 2010. Analysis of flow around impermeable groynes on one side of symmetrical compound channel: an experimental study. Water Sci. Eng. 3 (1), 56–66.
Armaly, B.F., Durst, F., Pereira, J., Schönung, B., 1983. Experimental and theoretical investigation of backward-facing step flow. J. Fluid Mech. 127, 473–496.
Aubry, N., 1991. On the hidden beauty of the proper orthogonal decomposition. Theor. Comput. Fluid Dyn. 2 (5–6), 339–352.
Berkooz, G., Holmes, P., Lumley, J.L., 1993. The proper orthogonal decomposition in the analysis of turbulent flows. Annu. Rev. Fluid Mech. 25 (1), 539–575.
Boyer, C., Roy, A.G., Best, J.L., 2006. Dynamics of a river channel confluence with discordant beds: flow turbulence, bed load sediment transport, and bed morphology. J. Geophys. Res.: Earth Surf. 111 (F4), F04007.
Brevis, W., García-Villalba, M., 2011. Shallow-flow visualization analysis by proper orthogonal decomposition. J. Hydraul. Res. 49 (5), 586–594.
Chen, K.K., Tu, J.H., Rowley, C.W., 2012. Variants of dynamic mode decomposition: boundary condition, koopman, and fourier analyses. J. Nonlinear Sci. 22 (6), 887–915.
Cheng, Z., Constantinescu, G., 2014. Spatial development of a constant-depth shallow mixing layer in a long channel. In: River Flow 2014. CRC Press 2014, p. 155.
Chrisohoides, A., Sotiropoulos, F., Sturm, T.W., 2003. Coherent structures in flat-bed abutment flow: computational fluid dynamics simulations and experiments. J. Hydraul. Eng. 129 (3), 177–186.
Chu, V.H., Babarutsi, S., 1988. Confinement and bed-friction effects in shallow turbulent mixing layers. J. Hydraul. Eng. 114 (10), 1257–1274.
Constantinescu, G., Sukhodolov, A., McCoy, A., 2009. Mass exchange in a shallow channel flow with a series of groynes: LES study and comparison with laboratory and field experiments. Environ. Fluid Mech. 9 (6), 587–615.
Duan, J.G., He, L., Fu, X., Wang, Q., 2009. Mean flow and turbulence around experimental spur dike. Adv. Water Resour. 32 (12), 1717–1725.
van der Graaf, G., 2010. GPIV, open source software for particle image velocimetry.
Francis, J., Pattanaik, A., Wearne, S., 1968. Technical note. observations of flow patterns around some simplified groyne structures in channels. Proc. Inst. Civ. Eng. 41 (4), 829–837.
Garde, R., Subramanya, K., Nambudripad, K., 1961. Study of scour around spur-dikes. J. Hydraul. Div. 86, 23–37.
Grift, R., Buijse, A., Van Densen, W., Machiels, M., Kranenbarg, J., Klein Breteler, J., Backx, J., 2003. Suitable habitats for 0-group fish in rehabilitated floodplains along the lower river rhine. River Res. Appl. 19 (4), 353–374.
Higham, J., Brevis, W., Keylock, C., 2016. A rapid non-iterative proper orthogonal decomposition based outlier detection and correction for PIV data. Meas. Sci. Technol. 27 (12), 125303.
Huang, H., Dabiri, D., Gharib, M., 1997. On errors of digital particle image velocimetry. Meas. Sci. Technol. 8 (12), 1427.
Jirka, G.H., Uijttewaal, W.S.J., 2004. Shallow flows: a definition. In: Shallow flows. A.A. Balkema Publishers, pp. 3–11.
Jovanović, M.R., Schmid, P.J., Nichols, J.W., 2014. Sparsity-promoting dynamic mode decomposition. Phys. Fluids (1994-present) 26 (2), 024103.
Kadota, A., Suzuki, K., 2010. Mean flow structure and advection of instantaneous coherent-flow pattern around t-type and l-type groynes. In: Environmental Hydraulics, Two Volume Set: Proceedings of the 6th International Symposium on Enviornmental Hydraulics, Athens, Greece, 23–25 June 2010. CRC Press, p. 81.
Karhunen, K., 1946. Zur spektral theorie stochastischer prozesse. Annales Academiæ Scientiarum Fennicæ A1:34.
Koken, M., 2011. Coherent structures around isolated spur dikes at various approach flow angles. J. Hydraul. Res. 49 (6), 736–743.
Koken, M., Constantinescu, G., 2008. An investigation of the flow and scour mechanisms around isolated spur dikes in a shallow open channel: 1. conditions corresponding to the initiation of the erosion and deposition process. Water Resour. Res. 44 (8), W08406.
Koken, M., Constantinescu, G., 2009. An investigation of the dynamics of coherent structures in a turbulent channel flow with a vertical sidewall obstruction. Phys. Fluids (1994-present) 21 (8), 085104.
Kosambi, D., 1943. Statistics in function space. J. Indian Math. Soc. 7, 76–88.
Le Clainche, S., Li, J.I., Theofilis, V., Soria, J., 2015. Flow around a hemisphere-cylinder at high angle of attack and low reynolds number. part i: experimental and numerical investigation. Aerosp. Sci. Technol. 44, 77–87.
Le Coz, J., Brevis, W., Niño, Y., Paquier, A., Riviére, N., 2006. Open-channel side-cavities: a comparison of field and flume experiments. In: River Flow 2006, Two Volume Set: Proceedings of the International Conference on Fluvial Hydraulics, Lisbon, Portugal, 6–8 September 2006. CRC Press, p. 145.
Loève, M., 1945. Functions aleatoire de second ordre. Comptes Rendus de l'Académie des Sciences 220.
Mezić, I., 2005. Spectral properties of dynamical systems, model reduction and decompositions. Nonlinear Dyn. 41 (1–3), 309–325.
Nadaoka, K., Yagi, H., 1998. Shallow-water turbulence modeling and horizontal large-eddy computation of river flow. J. Hydraul. Eng. 124 (5), 493–500.
Obukbov, A.M., 1954. Statistical description of continuous fields. Trudy Geofizicheskogo Instituta, Akademiya Nauk SSSR 24, 3–42.
Paik, J., Sotiropoulos, F., 2005. Coherent structure dynamics upstream of a long rectangular block at the side of a large aspect ratio channel. Phys. Fluids (1994-present) 17 (11), 115104.
Pougachev, V.S., 1953. General theory of the correlations of random functions. Izvestiya Akademii Nauk SSSR. Seriya Matematicheskaya. Bulletin de l'Académie des Sciences de l'URSS.
Przedwojski, B., 1995. Bed topography and local scour in rivers with banks protected by groynes. J. Hydraul. Res. 33 (2), 257–273.
Rempfer, D., Fasel, H.F., 1994. Evolution of three-dimensional coherent structures in a flat-plate boundary layer. J. Fluid Mech. 260, 351–375.
Rhoads, B.L., Sukhodolov, A.N., 2004. Spatial and temporal structure of shear layer turbulence at a stream confluence. Water Resour. Res. 40 (6), W06304.
Rowley, C.W., MEZIĆ, I., Bagheri, S., Schlatter, P., Henningson, D.S., 2009. Spectral analysis of nonlinear flows. J. Fluid Mech. 641, 115–127.
Ruhe, A., 1984. Rational krylov sequence methods for eigenvalue computation. Linear Algebra Appl. 58, 391–405.
Safarzadeh, A., Brevis, W., 2016. Assessment of 3d-RANS models for the simulation of topographically forced shallow flows. J. Hydrol. Hydromech. 64 (1), 83–90.
Safarzadeh, A., Salehi Neyshabouri, S.A.A., Zarrati, A.R., 2016. Experimental investigation on 3d turbulent flow around straight and t-shaped groynes in a flat bed channel. J. Hydraul. Eng. 8, 04016021.
Schmid, P.J., 2010. Dynamic mode decomposition of numerical and experimental data. J. Fluid Mech. 656, 5–28.
Schmid, P.J., 2011. Application of the dynamic mode decomposition to experimental data. Exp. Fluids 50 (4), 1123–1130.
Schmid, P.J., Meyer, K.E., Pust, O., 2009. Dynamic mode decomposition and proper orthogonal decomposition of flow in a lid-driven cylindrical cavity. In: 8th International Symposium on Particle Image Velocimetry-PIV09, pp. 1–4.
Socolofsky, S.A., Jirka, G.H., 2004. Large-scale flow structures and stability in shallow flows. J. Environ. Eng. Sci. 3 (5), 451–462.
Sukhodolov, A., Uijttewaal, W.S., Engelhardt, C., 2002. On the correspondence between morphological and hydrodynamical patterns of groyne fields. Earth Surf. Process. Landf. 27 (3), 289–305.
Sukhodolov, A.N., Rhoads, B.L., 2001. Field investigation of three-dimensional flow structure at stream confluences: 2. turbulence. Water Resour. Res. 37 (9), 2411–2424.
Sukhodolov, A.N., Schnauder, I., Uijttewaal, W.S., 2010. Dynamics of shallow lateral shear layers: experimental study in a river with a sandy bed. Water Resour. Res. 46 (11), W11519.
Talstra, H., 2011. Large-scale Turbulence Structures in Shallow Separating Flows. Ph.D. thesis. Technische Universiteit Delft.
Talstra, H., Uijttewaal, W.S., Stelling, G.S., 2006. Emergence of large-scale coherent structures in a shallow separating flow. In: Conference Proceedings of River Flow 2006, International Conference on Fluvial Hydraulics, Lisboa, pp. 261–269.
Tu, J.H., Rowley, C.W., Luchtenburg, D.M., Brunton, S.L., Kutz, J.N., 2013. On dynamic mode decomposition: theory and applications. arXiv preprint arXiv:1312.0041. arXiv preprint arXiv:1312.0041.
Uijttewaal, W., Tukker, J., 1998. Development of quasi two-dimensional structures in a shallow free-surface mixing layer. Exp. Fluids 24 (3), 192–200.
Uijttewaal, W.S., 2005. Effects of groyne layout on the flow in groyne fields: laboratory experiments. J. Hydraul. Eng. 131 (9), 782–791.
Wang, H., Gao, Q., Feng, L., Wei, R., Wang, J., 2015. Proper orthogonal decomposition based outlier correction for PIV data. Exp. Fluids 56 (2), 1–15.
Weitbrecht, V., Kühn, G., Jirka, G., 2002. Large scale PIV-measurements at the surface of shallow water flows. Flow Meas. Instrum. 13 (5), 237–245.
Wynn, A., Pearson, D., Ganapathisubramani, B., Goulart, P., 2013. Optimal mode decomposition for unsteady flows. J. Fluid Mech. 733, 473.

Please cite this article as: J.E. Higham et al., Using modal decompositions to explain the sudden expansion of the mixing layer in the wake of a groyne in a shallow flow, Advances in Water Resources (2017), http://dx.doi.org/10.1016/j.advwatres.2017.05.010